

Exclusion of multifold solutions of the CKM Unitarity Triangle by a time-dependent Dalitz plot analysis of $\bar{B}^0 \rightarrow D^{(*)0}h^0$ with $D^0 \rightarrow K_S^0\pi^+\pi^-$ decays combining BABAR and Belle data

Gerald Eigen (for the BABAR Collaboration)
 Department of Physics and Technology
 University of Bergen
 -5007 Bergen, NORWAY

Talk presented at the APS Division of Particles and Fields Meeting (DPF 2017), July 31-August 4, 2017, Fermilab. C170731.

Abstract

We present results of a new analysis campaign, which combines the final data samples collected by the B factory experiments *BABAR* and Belle in single physics analyses to achieve a unique sensitivity in time-dependent CP violation measurements. The data samples contain $(471 \pm 3) \times 10^6$ $B\bar{B}$ pairs recorded by the *BABAR* detector and $(772 \pm 11) \times 10^6$ $B\bar{B}$ pairs recorded by the Belle detector in e^+e^- collisions at the center-of-mass energies corresponding to the mass of the $\Upsilon(4S)$ resonance at the asymmetric-energy B factories PEP-II at SLAC and KEKB at KEK, respectively. We present a measurement of $\sin 2\beta$ and $\cos 2\beta$ by a time-dependent Dalitz plot analysis of $B^0 \rightarrow D^{(*)}h^0$ with $D \rightarrow K_S^0\pi^+\pi^-$ decays. A first evidence for $\cos 2\beta > 0$, the exclusion of trigonometric multifold solutions of the Unitarity Triangle and an observation of CP violation are reported.

1 Introduction

In the Standard Model, CP violation originates from the phase of the CKM matrix [1]. The unitarity relation $V_{ub}^*V_{ud} + V_{cb}^*V_{cd} + V_{tb}^*V_{td} = 0$ represents the so-called Unitarity Triangle (UT) illustrated in Fig. 1 (left). Sides $V_{ub}^*V_{ud}$, $V_{cb}^*V_{cd}$, $V_{tb}^*V_{td}$ and angles α, β, γ are extracted from many measurements in the B and K systems. At the B factories, $\sin 2\beta$ is measured in time-dependent CP asymmetries of $B^0 \rightarrow K^0c\bar{c}$ decays in which the $c\bar{c}$ forms a charmonium resonance [2]. The determination of β from $\sin 2\beta$ measurements leads to a two-fold ambiguity on 2β for $\eta < 90^\circ$, yielding $\beta = 21.9^\circ$ and $\beta = \pi/2 - 21.9^\circ = 68.1^\circ$ as shown in Fig. 1 (right) [3]. To lift this ambiguity, a measurement of $\cos 2\beta$ is necessary.

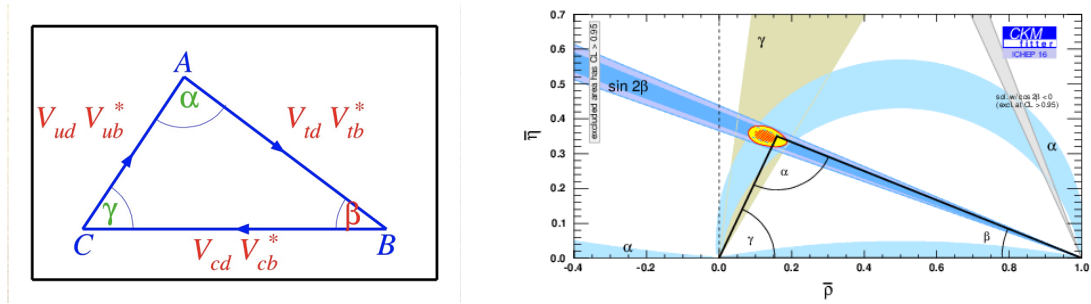


Figure 1: Graphical representation of the Unitarity Triangle defining the sides $V_{ub}^*V_{ud}$, $V_{cb}^*V_{cd}$, $V_{tb}^*V_{td}$ and angles α, β, γ (left). Present status of the Unitarity Triangle showing the two solutions of $\beta = 21.9^\circ$ and $\beta = 68.1^\circ$ (right).

2 Analysis Methodology

We perform a time-dependent Dalitz plot analysis of $\bar{B}^0 \rightarrow D^{(*)0}h^0$ with $D^0 \rightarrow K_S^0\pi^+\pi^-$ decays and where h^0 represents a $\pi^0 \rightarrow \gamma\gamma, \eta \rightarrow \gamma\gamma, \pi^+\pi^-\pi^0$ or $\omega \rightarrow \pi^+\pi^-\pi^0$. Figure 2 shows the lowest-order Feynman diagrams. The $b \rightarrow \bar{c}ud$ tree dominates whereas the contribution from the doubly-CKM suppressed tree $b \rightarrow \bar{u}cd$ is small. The tree amplitudes interfere with the amplitude of corresponding \bar{B}^0 decay that is produced via $B^0\bar{B}^0$ mixing. Thus, the absolute amplitudes squared for B^0 and \bar{B}^0 decay are [4]

$$|M_{B^0}(\Delta t)|^2 = |\mathcal{A}_{\bar{D}^0} \times \cos(\frac{1}{2}\Delta m\Delta t) - ie^{+2i\beta} \times \mathcal{A}_{D^0} \times \sin(\frac{1}{2}\Delta m\Delta t)|^2 \quad (1)$$

$$|M_{\bar{B}^0}(\Delta t)|^2 = |\mathcal{A}_{D^0} \times \cos(\frac{1}{2}\Delta m\Delta t) - ie^{-2i\beta} \times \mathcal{A}_{\bar{D}^0} \times \sin(\frac{1}{2}\Delta m\Delta t)|^2,$$

where $\mathcal{A}_{\bar{D}^0}$ and \mathcal{A}_{D^0} are the amplitudes of the $\bar{D}^0 \rightarrow K_S^0\pi^+\pi^-$ and $D^0 \rightarrow K_S^0\pi^+\pi^-$ decays. The interference of the \bar{D}^0 and the D^0 in the Dalitz plot introduce a dependence on $\cos 2\beta$. Belle previously measured $\cos 2\beta = 1.05 \pm 0.33_{-0.15}^{+0.21}$ [5]. By combining BABAR and Belle data consisting of a total luminosity of 1.1 ab^{-1} , the sensitivity to $\cos 2\beta$ is greatly improved. The first step is to develop a Dalitz plot model for $D^0 \rightarrow K_S^0\pi^+\pi^-$ decay followed by the extraction of the $\bar{B}^0 \rightarrow D^{(*)0}h^0$ signal for which a time-dependent CP analysis is performed.

2.1 $D^0 \rightarrow K_S^0\pi^+\pi^-$ Dalitz Plot Amplitude Model

The $D^0 \rightarrow K_S^0\pi^+\pi^-$ Dalitz plot model was built using Belle $e^+e^- \rightarrow c\bar{c}$ data. The D^0 is produced in the decay $D^{*+} \rightarrow D^0\pi_s^+$. The charge of the slow π_s^+ determines

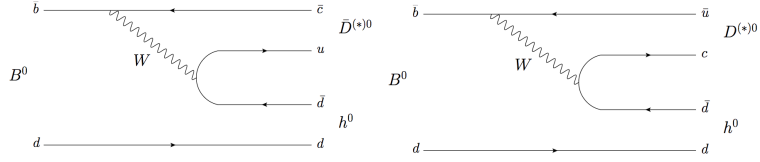


Figure 2: Lowest-order tree diagram (left) and doubly-CKM-suppressed tree diagram (right) for $\bar{B}^0 \rightarrow D^{(*)0} h^0$ with $D^0 \rightarrow K_S^0 \pi^+ \pi^-$ decays.

the flavor of the D^0 . To remove background from B decays, we require the candidate momentum for decays in the $\Upsilon(4S)$ ($\Upsilon(5S)$) center-of-mass systems to satisfy $p^*(D^{*+}) > 2.5$ (3.1) GeV. We determine D^{*+} decay vertex with a kinematic fit for the D^0 daughter with the constraint to originate from the e^+e^- interaction region. Furthermore, we require that the slow π_s^+ originates from the D^{*+} decay vertex to improve the resolution of the $D^{*+} - D^0$ mass difference. We then extract $D^{*+} \rightarrow D^0 \pi_s^+$ yield from a two-dimensional fit to the D^0 mass and $D^{*+} - D^0$ mass difference. Figure 3 shows the scatter plot of the D^0 mass versus the $D^{*+} - D^0$ mass difference. We obtain a yield of 1.22 million signal events in the region of $144.4 < M_{D^*} - M_D < 146.4$ MeV and $1850 < M_{D^0} < 1880$ MeV with a purity of 94%.

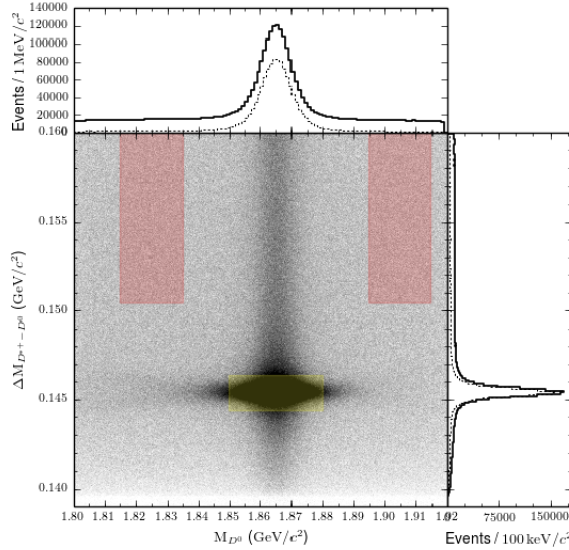


Figure 3: Scatter plot of the $D^{*+} - D^0$ mass difference versus the D^0 mass and its projections. The yellow and red bands show the signal and sideband regions, respectively. The dashed lines indicate the signal contributions.

We fit the $D^0 \rightarrow K_S^0 \pi^+ \pi^-$ Dalitz plot with isobars accounting for 13 intermediate two-body resonances and $K\pi$ and $\pi\pi$ S-waves where the S-waves are modelled by the

LASS [8] and K-matrix [7] parameterizations, respectively.

$$\mathcal{A}_{D^0}(m_+^2, m_-^2) = \sum_{r \neq (K\pi, \pi\pi)_{L=0}} a_r e^{i\phi_r} \mathcal{A}_r(m_+^2, m_-^2) + \mathcal{A}_{(k\pi)_{L=0}}(s) + F_1(s) \quad (2)$$

The intermediate resonances are parametrized in terms of magnitude a_r , phase ϕ_r and amplitude $\mathcal{A}_r(m_+^2, m_-^2)$. The latter is factorized in terms of the Zemach tensor (Z_L) [9] describing the angular distribution of final state, Blatt-Weisskopf barrier penetration factors for the D meson (F_D) and the resonance (F_r) as well as a propagator (T_r) describing the decay dynamics of the resonances parameterized by Breit-Wigner functions. The isobar model includes Cabibbo-allowed two-body resonances ($K^*(890)^-$, $K_0^*(1430)^-$, $K_2^*(1430)^-$, $K^*(1680)^-$ and $K^*(1410)^-$), doubly-CKM-suppressed states ($K^*(890)^+$, $K_0^*(1430)^+$, $K_2^*(1430)^+$, and $K^*(1410)^+$) as well as CP eigenstates ($\rho(770)$, $\omega(782)$, $f_2(1270)$ and $\rho(1450)$). We perform a Dalitz plot fit for flavor-tagged events in the signal region with a correction for efficiency variations in Dalitz plot phase space. We take background from the D^0 mass and $D^{*+} - D^0$ mass difference sidebands. The free parameters in the fit are a_r and ϕ_r of each resonance relative to those of the ρ ($a_\rho = 1$ and $\phi_\rho = 0$), the LASS and K-matrix parameters plus masses and widths of the $K^*(892)$ and $K^*(1430)$. Figure 4 shows the Dalitz plot and its three projections for the Belle $c\bar{c}$ sample with fit results overlaid. The $K^*(892)$ is the dominant resonance. It is clearly visible in the Cabibbo-allowed Dalitz plot projection and appears as reflections at 1.2 GeV² and 2.5 GeV² in the doubly-CKM suppressed projection.

2.2 Extraction of the $\bar{B}^0 \rightarrow D^{(*)0} h^0$ signal yield

In total, we reconstruct five \bar{B}^0 decay modes ($D^0\pi^0$, $D^0\eta$, $D^0\omega$, $D^{*0}\pi^0$ and $D^{*0}\eta$) in which the D^0 , D^{*0} and neutral hadron h^0 are reconstructed in the decays $D^0 \rightarrow K_S^0\pi^+\pi^-$, $D^{*0} \rightarrow D^0\pi^0$, and ($\eta^0 \rightarrow \gamma\gamma$, $\eta \rightarrow \gamma\gamma$ or $\eta \rightarrow \pi^+\pi^-\pi^0$ and $\omega \rightarrow \pi^+\pi^-\pi^0$). We introduce a transformed beam-constrained mass, M'_{bc} , to remove the correlation between the energy difference $\Delta E = E_B^* - E_{beam}^*$ ¹ and M_{bc}

$$M'_{bc} = \sqrt{E_{beam}^{*2} - (\vec{p}_{D^{(*)}0}^* + \frac{\vec{p}_{h^0}^*}{|\vec{p}_{h^0}^*|} \sqrt{(E_{beam}^* - E_{D^{(*)}0}^*)^2 - M_{h^0}^2})}. \quad (3)$$

To separate signal from $e^+e^- \rightarrow q\bar{q}$ continuum background (with $q = u, d, s, c$ quarks), we define a transferred neural network output variable

$$NN'_{out} = \log \frac{NN_{out} - NN_{out}^{min}}{NN_{out}^{max} - NN_{out}} \quad (4)$$

¹where E_b^* is the B-meson energy and E_{beam}^* is the beam energy where an asterisk denotes that these observables are measured in the e^+e^- center-of-mass frame

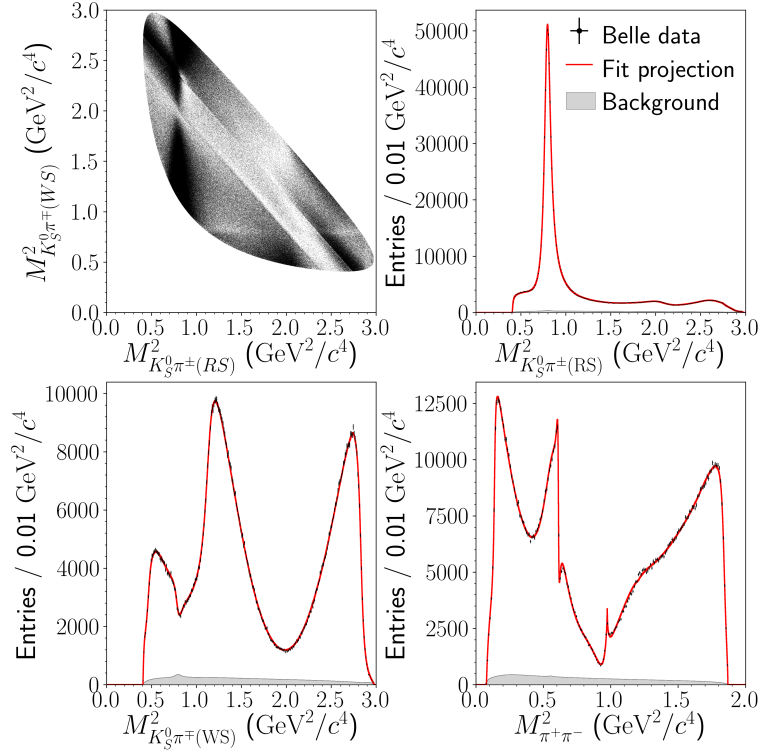


Figure 4: The $M_{K_S^0 \pi^\pm}^2$ versus $M_{K_S^0 \pi^\mp}^2$ Dalitz plot and the $M_{K_S^0 \pi^\pm}^2$, $M_{K_S^0 \pi^\mp}^2$ and $M_{\pi^+ \pi^-}^2$ projections for Belle data with fits results overlaid. The residual 6% $c\bar{c}$ background is represented by the grey-shaded distribution.

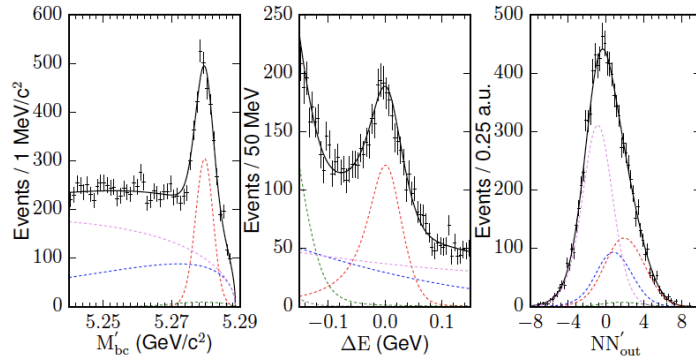


Figure 5: Distributions of M'_{bc} (left), ΔE (middle) and NN'_{out} (right) showing data (points), total fit (black line), signal (red dashes), combinatorial background (blue dashes), continuum background (magenta dashes) and cross-feed (green dashes).

The neural network variable NN_{out} combines event shape information from 16 modified Fox-Wolfram moments. We perform a coherent analysis strategy, applying essentially the same selection criteria on *BABAR* and Belle data. We extract signal yields from three-dimensional fits to M'_{bc} , ΔE and NN'_{out} . For each mode in each experiment we perform separate fits using the experiment-specific resolutions. Figure 5 shows the distributions for M'_{bc} , ΔE and NN'_{out} with fit projections overlaid after combining all five modes for both experiments. The three-dimensional fits describe the data rather well. We obtain 1129 ± 48 *BABAR* and 1567 ± 56 Belle signal events. Table 1 lists the yields for the individual modes in the two experiments.

Decay mode	<i>BABAR</i>	Belle
$\bar{B}^0 \rightarrow D^0 \pi^0$	469 ± 31	768 ± 37
$\bar{B}^0 \rightarrow D^0 \eta$	220 ± 22	238 ± 23
$\bar{B}^0 \rightarrow D^0 \omega$	219 ± 21	285 ± 26
$\bar{B}^0 \rightarrow D^{*\pi^0}$	147 ± 18	182 ± 19
$\bar{B}^0 \rightarrow D^{*\eta}$	74 ± 11	94 ± 13

Table 1: Individual signal yields per decay mode and experiment.

3 Time-dependent CP analysis

We fit the proper time interval distributions maximizing the log-likelihood function

$$\ln \mathcal{P} = \sum_i \ln \mathcal{P}_i^{BABAR} + \sum_j \ln \mathcal{P}_j^{Belle}. \quad (5)$$

The physics probability density functions (pdf) \mathcal{P}_i^{BABAR} and \mathcal{P}_j^{Belle} are convolved with experiment-specific resolution functions

$$\mathcal{P}_{\text{exp}} = \sum_k f_k \int [\mathcal{P}_k(\Delta t) R_k(\Delta t - \Delta t')] d\Delta t'. \quad (6)$$

We apply the *BABAR*- and Belle-specific flavor-tagging algorithms and a common signal model for both experiments. The signal pdf is obtained from eqn 1.

$$\begin{aligned} \mathcal{P}_{\text{sig}} \propto & [|\mathcal{A}_{\bar{D}^0}|^2 + |\mathcal{A}_{D^0}|^2] \mp [|\mathcal{A}_{\bar{D}^0}|^2 - |\mathcal{A}_{D^0}|^2] \cos(\Delta m \Delta t) \\ & \pm 2\eta_{h^0} (-1)^L [Im(\mathcal{A}_{D^0} \mathcal{A}_{\bar{D}^0}^*) \cos 2\beta - Re(\mathcal{A}_{D^0} \mathcal{A}_{\bar{D}^0}^*) \sin 2\beta] \sin(\Delta m \Delta t) \end{aligned} \quad (7)$$

The B^0 and B^+ lifetimes and the $B^0 \bar{B}^0$ mixing parameter Δm_d are fixed to the world averages [12], while the Dalitz plot amplitude model parameters are fixed to the fit results of the $D^0 \rightarrow K_S^0 \pi^+ \pi^-$ Dalitz plot analysis. The only free parameters in the fit are $\sin 2\beta$ and $\cos 2\beta$.

4 Results

Using 1.1 ab^{-1} of *BABAR* and Belle data we measure:

$$\sin 2\beta = 0.80 \pm 0.14_{\text{stat}} \pm 0.06_{\text{sys}} \pm +0.03_{\text{model}} \quad (8)$$

$$\cos 2\beta = 0.91 \pm 0.22_{\text{stat}} \pm 0.09_{\text{sys}} \pm +0.07_{\text{model}} \quad (9)$$

$$\beta = (22.5 \pm 4.4_{\text{stat}} \pm 1.2_{\text{sys}} \pm 0.6_{\text{model}})^\circ \quad (10)$$

We observe *CP* violation in the decay $\bar{B} \rightarrow D^{(*)}h^0$ in the time-dependent decay distributions as expected in the Standard Model. The value of $\sin 2\beta$ is in good agreement with the world average of 0.69 ± 0.02 [11]. Our results yield the first evidence for $\cos 2\beta > 0$ at 3.7 standard deviations. The second solution of $\beta = (68.1 \pm 0.7)^\circ$ is excluded at 7.3 standard deviations thus removing the ambiguity in extracting β from $\sin 2\beta$. In addition, $\beta = 0$ is excluded at 5.1 standard deviations. Figure 6 shows the $2\Delta \ln L$ distributions as functions of $\sin 2\beta$, $\cos 2\beta$ and β .

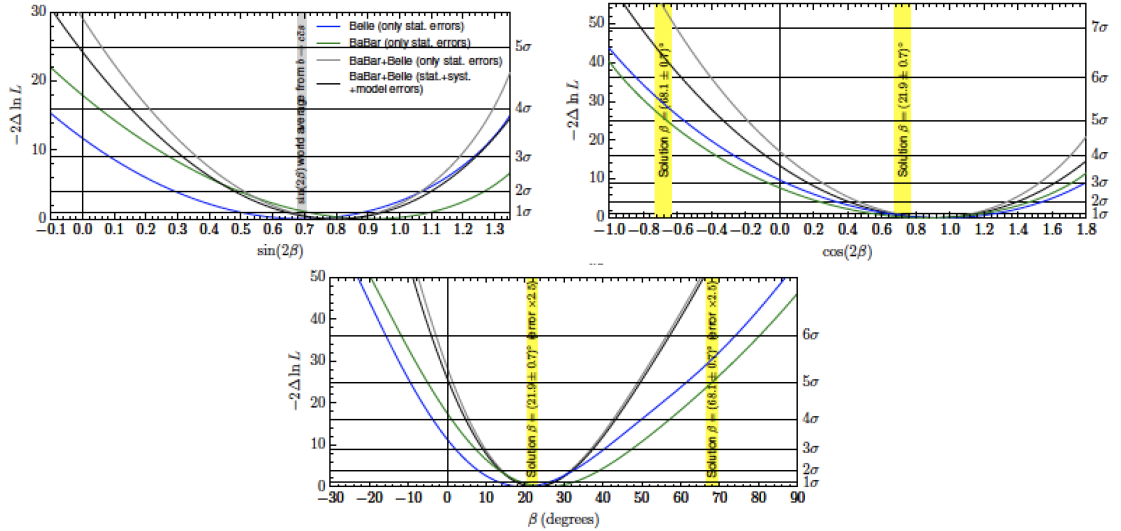


Figure 6: The $2\Delta \ln L$ distributions as functions of $\sin 2\beta$ (top left), $\cos 2\beta$ (top right) and β (bottom) for *BABAR* data (green line), Belle data (blue line) and both experiments combined (grey line) using statistical errors only. The result for both experiments including systematic uncertainties are shown by the black solid curves.

5 Systematic uncertainties

Table 2 shows the experimental systematic uncertainties on the *CP* violation parameters. The largest systematic errors on $\cos 2\beta$ result from the uncertainties in

the Δt resolution functions (0.058), followed by those in the vertex reconstruction, possible fit bias and signal purity. Systematic uncertainties from the background Δt pdfs are smaller while those from flavor tagging, physics parameters and Dalitz plot reconstruction efficiency corrections are negligible.

Source	$\sin 2\beta[\times 10^2]$	$\cos 2\beta[\times 10^2]$	$\beta[^\circ]$
Δt resolution functions	2.84	5.75	0.41
Vertex reconstruction	3.16	4.79	0.53
Possible fit bias	3.67	3.90	0.79
Signal purity	2.13	3.39	0.53
Background Δt pdfs	1.24	1.76	0.16
Flavor tagging	0.34	0.39	0.07
Dalitz plot reconstruction efficiency correction	0.01	0.17	0.02
Physics parameters	0.07	0.14	0.02
Total	6.14	9.27	1.18

Table 2: Summary of experimental systematic uncertainties on the CP violation parameters.

6 Conclusions

We have performed a time-dependent CP analysis of the decay mode $\bar{B}^0 \rightarrow D^{(*)0}h^0$ where the D^0 is reconstructed in the $K_S^0\pi^+\pi^-$ final state using 1.1 ab^{-1} of *BABAR* and Belle data. We measure $\cos 2\beta = 0.91 \pm 0.22_{\text{stat}} \pm 0.09_{\text{sys}} \pm 0.07_{\text{model}}$ from which we exclude the solution $\beta = (68.1 \pm 0.7)^\circ$ at 7.3 standard deviations. Our measurement lifts the ambiguity in the determination of the angle β in the Unitarity Triangle. Our result for β agrees well with the world average which is shown in Fig. 7 in comparison to a previous measurement of β in the decay mode $\bar{B}^0 \rightarrow D_{CP}h^0$ using combined *BABAR* and Belle data.

7 Acknowledgment

I would like to thank the *BABAR* collaboration for the opportunity to present these results. In particular I would like to thank M. Röhrken, J. McKenna and F.C. Porter for useful discussion.

$$\mathbf{b} \rightarrow \mathbf{c} \bar{u} d \quad \sin(2\beta) \equiv \sin(2\phi_1) \quad \text{HFLAV Summer 2016}$$

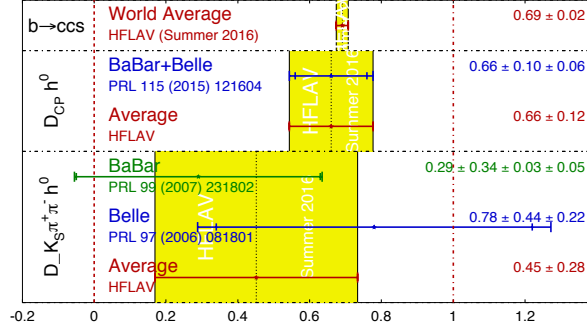


Figure 7: Compilation of $\sin 2\beta^{eff}$ measurement in time dependent $b \rightarrow \bar{c} u d$ analyses before the recent measurement [6, 13, 14].

References

- [1] N. Cabibbo, Phys. Rev. Lett. 10, 531 (1963); M. Kobayashi and T. Maskawa, Prog. Theor. Phys. 49, 652 (1973).
- [2] The BABAR Collaboration (B. Aubert *et al.*), Phys.Rev.D79, 072009 (2009); the Belle Collaboration (I.Adachi *et al.*), Phys. Rev. Lett. 108, 171802 (2012).
- [3] CKMfitter Group (J.Charles *et al.*), <http://ckmfitter.in2p3.fr/>
- [4] A. Bondar, T. Gershon, and P. Krokovny, Phys. Lett. B624, 1 (2005).
- [5] The Belle Collaboration (V. Vorobyev *et al.*), Phys. Rev. D 94, 052004 (2016).
- [6] The BABAR and Belle Collaborations (A. Abdesselam, I. Adachi, A. Adametz *et al.*), Phys. Rev. Lett.115, 121604 (2015).
- [7] S.U. Chung *et al.*, Annalen der Physik, 507, 404 (1995); I. Aitchison, Nucl. Phys. A 189, 417 (1972).
- [8] The LASS Collaboration (D. Aston *et al.*), Nucl. Phys. B 296, 493 (1988).
- [9] C. Zemach, Phys. Rev., 140 B, 97 (1965).
- [10] The BABAR Collaboration (B. Aubert *et al.*), Phys.Rev.D78, 034023 (2008).
- [11] Heavy Flavor Averaging Group, <http://www.slac.stanford.edu/xorg/hfag/>.
- [12] K.A. Olive et al. (Particle Data Group), Chin. Phys. C 38, 090001 (2014).
- [13] The BABAR Collaboration (B. Aubert *et al.*), Phys. Rev. Lett. 99, 231802 (2007).
- [14] The Belle Collaboration (P. Krokovny *et al.*), Phys. Rev. Lett. 97, 081801 (2006).